International Journal of Pharmaceutics 422 (2012) 472–478

Contents lists available at SciVerse ScienceDirect

International Journal of Pharmaceutics

journal homepage: www.elsevier.com/locate/ijpharm

Pharmaceutical nanotechnology

# Synthesis and biological evaluation of radiolabeled photosensitizer linked bovine serum albumin nanoparticles as a tumor imaging agent

Aykut Ozgur[a], Fatma Yurt Lambrecht[a,*], Kasim Ocakoglu[b], Cumhur Gunduz[c], Musteyde Yucebas[c]

[a] Department of Nuclear Applications, Institute of Nuclear Science, Ege University, Bornova TR-35100, Izmir, Turkey
[b] Advanced Technology Research & Application Center, Mersin University, Ciftlikkoy Campus, TR-33343 Yenisehir, Mersin, Turkey
[c] Department of Medical Biology, Faculty of Medicine, Ege University, Bornova TR-35100, Izmir, Turkey

ARTICLE INFO

*Article history:*
Received 10 August 2011
Received in revised form 13 October 2011
Accepted 6 November 2011
Available online 15 November 2011

*Keywords:*
BSA nanoparticles
Pheophorbide-a
Drug delivery systems
MCF-7
$^{99m}$Tc

ABSTRACT

In this study, we reported on the synthesis and biological evaluation of radiolabeled fluorescent dye conjugated bovine serum albumin nanoparticles within the size range 190–210 nm. The bovine serum albumin nanoparticles (BSANPs) were prepared using a desolvation method, and chemical cross-linking was performed using gluteraldehyde. Furthermore, pheophorbide-a (PH-A) was loaded on the BSANPs. The results obtained from dynamic light scattering and electron microscopy have proved that nanoparticles are highly monodisperse and near-spherical shaped. The photo-physical properties of the PH-A-BSANPs were obtained using the spectrophotometric techniques. According to the results, PH-A and BSANPs show high non-covalent interaction. PH-A loaded nanoparticles were labeled with $^{99m}$Tc and the radiolabeling efficiency was determined as 90 ± 1.2%. Biodistribution studies of $^{99m}$Tc labeled PH-A-BSANPs and PH-A were carried out using female Albino Wistar rats, and $^{99m}$Tc-PH-A-BSANPs showed a significantly higher uptake in the breast and uterus than $^{99m}$Tc-PH-A. Cell culture study was carried out in MCF-7 cell line (human breast adenocarcinoma cell line). According to the cell culture studies, $^{99m}$Tc-PH-A-BSANPs showed a higher uptake than $^{99m}$Tc-PH-A. Moreover, PH-A-BSANPs demonstrated good photo-physical properties and BSANPs increased the uptake of PH-A on to the MCF-7 cell line. These results confirm that $^{99m}$Tc labeled PH-A-BSANPs could be utilized for radioimaging.



## 1. Introduction

Recent advances in nanotechnology have stimulated novel applications in cancer therapy and diagnosis where nanoparticles are used to achieve colloidal drug delivery systems. The major goals of in colloidal drug delivery systems are controlled transport of the drug to target cells and tissues at a therapeutically optimal rate and dose regimen. Thus, they can prevent the unwanted toxic side effects of the drug and improve its therapeutic effects (Crommelin and Schreier, 1994; Zhang et al., 2004; Hans and Lowman, 2002). Nanoparticles are useful drug delivery systems for the selective transport of the drug to the target cells and tissues. Therefore, they may be combined with targeting ligand, imaging-probes and polymers via adsorption or conjugation (Wang et al., 2010; Yang et al., 2010; Lin et al., 1999; Cho et al., 2008).

Nanoparticles can be prepared using a variety of materials such as proteins, synthetic polymers and lipids. The selection of materials is dependent on size and surface characteristics, toxicity, and the biodegradability of nanoparticles (Wang et al., 2010; Mohanraj and Chen, 2006). Among polymer materials, those based on proteins are particularly preferred such as serum albumin and gelatin, which are widely used for the preparation of nanoparticles in drug delivery systems (Ofokansi et al., 2010; Labhasetwar et al., 1996). Since, they are non-toxic, biodegradable, easy to prepare, and their size distribution can be easily monitored. Moreover, proteins have some functional groups such as amino, carboxylic and hydroxyl, and these groups make easy the bonding process between drug and protein based nanoparticles through covalent linking and non-covalent adsorption (Weber et al., 2000).

Nanoparticulate colloid systems have been improved for the diagnosis of cancer. For example, strong fluorescence emitting materials, super-paramagnetic iron oxide (SPIO) and gadolinium chelates are loaded on the nanoparticles for the imaging of target tumors (Yang et al., 2010). One different approach for tumor imaging is to use radiolabeled ($^{99m}$Tc, $^{67}$Ga, $^{111}$In etc.) agent conjugated nanoparticles such as hematoporphyrin derivatives and porphyrin analogues bearing albumin nanoparticles. These agents demonstrate good localization in tumors, and they can easily form a complex with radionuclide for having chelating properties (Yang et al., 2010; Babbar et al., 2000; Josefsen and Boyle, 2007; Murugesan et al., 2002). Furthermore, many photosensitizer compounds exhibit hydrophobic characteristics, thus they can be

* Corresponding author. Tel.: +90 232 311 50 17; fax: +90 232 388 64 66.
*E-mail address:* fatma.yurt.lambrecht@ege.edu.tr (F.Y. Lambrecht).

0378-5173/$ – see front matter © 2011 Elsevier B.V. All rights reserved.
doi:10.1016/j.ijpharm.2011.11.013

combined with nanoparticles for effective distribution in the body (Chatterjee et al., 2008).

Albumin is a major protein in blood plasma, and it has a great potential as a nanocarrier in drug delivery systems. It is widely used in nanoparticulate colloid systems due to its non-toxic and biodegradable properties. Many organic and inorganic molecules can interact easily with albumin nanoparticles owing to their proper functional groups on the particle surface. In addition, albumin is a protein which is soluble, and stable in a wide range of pH and up to 60 °C. So, it is a suitable protein for preparing nanoparticles, which are widely used in colloidal drug delivery systems (Chen et al., 2009; Kratz, 2008; Sharman et al., 2004). The desolvation process is commonly used to prepare polymer based nanoparticles such as BSANPs. The addition of desolvating agents such as ethanol causes a better controlled separation and precipitation of the particles (Jun et al., 2011).

Chlorophyll derivatives are colored compounds and possess well-known naturally occurring photosensitizing properties. PH-A is synthesized from chlorophyll-*a* by the elimination of phytol and magnesium (Keller et al., 1996). PH-A is an efficient photosensitizer agent and extensively used in photodynamic therapy. Previous research results demonstrated that PH-A can be used for the treatment of a number of tumors and microbial infections. It has been considered as for anti-tumor and anti-inflammatory agents. Some photosensitizers (T3, 4BCPC, Photosan-3) like PH-A were labeled with $^{99m}$Tc and their potential for murine tumors was evaluated, and it was found useful for monitoring cancer (Chen et al., 2009; Jori et al., 2006; Aprahamian et al., 1993). On the other hand PH-A was labeled with Tc-99m by Ocakoglu et al. and its potential was evaluated in infection imaging (Ocakoglu et al., 2011).

Recently, numerous photosensitizer linked albumin nanoparticles have been synthesized and evaluated for tumor imaging and PDT. However, in this paper PH-A was prepared from a biological material, and it was loaded on protein based nanoparticles. The generated structure is commonly natural, and it was prepared using easy synthesis methods. Due to all these important advantages of PH-A, in current study, bovine serum albumin nanoparticles (BSANPs) was prepared using a desolvation technique, and PH-A was loaded on BSANPs by non-covalent adsorption. Then, BSANPs-PH-A nanoparticles were labeled with $^{99m}$Tc. Additionally, the radiopharmaceutical potential of radiolabeled photosensitizer linked bovine serum albumin nanoparticles was examined in female Albino Wistar rats and MCF-7 cells.

## 2. Materials and methods

### 2.1. Materials

$^1$H NMR measurements were performed on a Bruker 400 MHz spectrometer using residual solvent peaks as internal standards. Absorption spectra were recorded on a 1 cm path length quartz cell on a Shimadzu UV-2102 UV–vis spectrophotometer. Mass analysis was performed using a Waters LCT Premier (ESI).

Bovine serum albumin (BSA) was supplied by Sigma Aldrich Chemical Co. (Steinheim am Albuch, Germany). The RPMI 1640, Trypsin-EDTA, fetal bovine serum, L-glutamine, penicillin and streptomycin were from Biological Industries Ltd. (Haemek, Israel). The WST-1 reagent (2-(4-iodophenyl)-3-(4-nitrophenyl)-5-(2,4-disulfophenyl)-2H-5-tetrazolium, monosodium salt) was from Roche. MCF-7 (a human breast adenocarcinoma cell line) was obtained from the Department of Medical Biology, Ege University. $Na^{99m}TcO_4$ was supplied by the Department of Nuclear Medicine, Ege University, as an eluent of $^{99}$Mo/$^{99m}$Tc generator (Monrol, Istanbul, Turkey). Analytical grade glutaraldehyde (50% solution), ethanol and other reagents were purchased from Merck Chemical Co. (Darmstadt, Germany).

### 2.2. Synthesis of pheophorbide-a (PH-A)

The PH-A (methyl 13$^2$-demethoxycarbonylpheophorbide-a) was synthesized from chlorophyll-*a*, which was isolated from *Spirulina maxima* algae, according to a known literature procedure (Smith et al., 1985; Huber et al., 2008). Starting with 500 g of algae, approximately 2 g of PH-A was obtained, and then the synthesized product was characterized by NMR, UV–vis spectrophotometer and mass spectrometry.

### 2.3. Preparation of BSA nanoparticles

The desolvation technique was used for preparation of BSA nanoparticles (BSANPs). BSA (200 mg) was dissolved in 2 mL of distilled water. Ethanol (8 mL) was added a drop by drop with a pump controlled system (1 mL/min) into the 10% BSA solution stirring continuously. After the desolvation process, 235 μL of 8% glutaraldehyde solution in water was added to the solution (10% BSA) to carry out the particle cross-linking. The cross-linking was performed by continuous stirring of the suspension over a time period of 24 h at room temperature (Langer et al., 2003). The suspension was centrifuged and the pellets were solidified by a freeze-drying process.

### 2.4. Preparation of PH-A-BSANPs

The PH-A was loaded onto the BSA nanoparticles by non-covalent drug adsorption. The BSANPs (27.89 mg) were dispersed in distilled water (1 mL), and 60 μg PH-A (from the solution of 1 mg/mL PH-A in ethanol) was added to the suspension. And the suspension was mixed using a magnetic stirrer for 5 min. Then the suspension was adjusted to 2 mL with distilled water, and it was incubated for 10 min by ultrasonication at room temperature (Chen et al., 2009). After the adsorption process, the optical property of the PH-A-BSANPs was evaluated using steady-state fluorescence and UV–vis absorption spectroscopy.

### 2.5. Characterization of BSANPs and PH-A-BSANPs

#### 2.5.1. Determination of particle size, zeta potential and morphology

The particle size, zeta potential and morphology of the BSANPs and PH-A-BSANPs were measured using dynamic light scattering (DLS) (Malvern Zetasizer Nano ZS, Malvern, UK) and scanning electron microscope (SEM) (FEI Quanta250 FEG) instruments. For the measurement of DLS, the particles were dispersed in distilled water and measured at a scattering angle of 90° at room temperature. In order to obtain SEM images, the nanoparticles were solidified by a freeze-drying process, and then the solid nanoparticles were put on the surface of special mica discs.

#### 2.5.2. Steady-state fluorescence and UV–vis absorption spectroscopy

The photophysical properties of the PH-A and PH-A-BSANPs were investigated by UV–vis absorption and fluorescence emission spectroscopy. The steady-state fluorescence emission spectra of the PH-A and PH-A-BSANPs were recorded using a Varian Cary 50 spectrophotometer ($\lambda_{ex}$: 514 nm) in ethanol at room temperature.

After the adsorption process, the PH-A-BSANPs were washed three times, and UV–vis absorption measurements were taken at 670 nm for each wash-water. The efficiency of adsorption of PH-A onto BSANPs was determined in respect of the results.

### 2.6. Radiochemical synthesis of $^{99m}$Tc-PH-A and $^{99m}$Tc-PH-A-BSANPs

The PH-A was labeled with $^{99m}$Tc according to the stannous (II) chloride method. The PH-A (1 mg) was dissolved in 1 mL ethanol and mixed with 100 μL $SnCl_2{\cdot}2H_2O$ (1 mg/mL) in the vial. 37–74 MBq $Na^{99m}TcO_4$ was slowly added and the mixture was incubated at 60–70 °C in a water bath for 25 min (Langer et al., 2003). The radiochemical efficiency of $^{99m}$Tc-PH-A was determined using thin layer chromatography. $^{99m}$Tc-PH-A was spotted onto aluminum-coated plastic sheets (1 cm × 10 cm) (Merck 5565) and developed in two different mobile phases, depending upon the chromatographic method. The first mobile phase was ACD (citrate-dextrose buffer solution), and the second one was methanol/water (80/20) (Ocakoglu et al., 2011). After developing, the sheets were dried. Then, they were scanned using a BioScan TLC-scanner (Bioscan AR-2000 Washington DC). The $R_f$ values and labeling efficiency of $^{99m}$Tc-PH-A were then determined.

Radiolabeling of PH-A-BSANPs with $^{99m}$Tc was performed according to labeling procedure of PH-A. After labeling procedure, $^{99m}$Tc-PH-A-BSANPs were washed three times. Each washing process, $^{99m}$Tc-PH-A-BSANPs and supernatant were counted with Cd(Te) detector. Consequently, the radiolabeling efficiency was determined.

The stability of $^{99m}$Tc-PH-A-BSANPs was tested in a pH 7 phosphate buffer solution (PBS) at 37 °C shaken continuously. Sample (500 μL) was taken from the upper phase at 30, 60, 90, 120 min and its radioactivity was counted using a Cd(Te) RAD 501 single channel analyzer. In this process, the radioactivity of $^{99m}$Tc in upper phase was counted, and the temporal stability of $^{99m}$Tc-PH-A-BSANPs was calculated.

### 2.7. Biodistribution study on rats

The protocol was approved by the Animal Ethics Committee of Ege University. Biodistribution studies were performed using female healthy Albino Wistar rats (body mass 200–220 g). $^{99m}$Tc-PH-A-BSANPs (specific activity: 10.24 GBq/μmol/rat) and $^{99m}$Tc-PH-A (specific activity: 0.88–1.76 GBq/μmol/rat) were injected the tail vein of the rats. The rats were sacrificed under intense ether atmosphere at 30, 60 and 120 min post injection. The organs and tissues (kidneys, large intestine, ovary, breasts and uterus) were excised, weighed and their radioactivity was counted using a Cd(Te) RAD 501 single channel analyzer. The results were expressed as a percentage injected dose per gram of each organ (%ID/g) for various selected organs as the mean value of the rats. In this biodistribution study, three rats were used for each time point.

### 2.8. Cell culture studies on MCF-7 cell line

Cell uptake studies were carried out using a MCF-7 cell line, a human breast adenocarcinoma cell model. The cells were grown in T-75 flasks as a monolayer at 37 °C in a 5% $CO_2$ humidified incubator using RPMI-1640 medium with 10% fetal bovine serum, 1% L-glutamine, 100 IU/mL penicillin and 10 mg/mL streptomycin.

#### 2.8.1. Cytotoxicity assay of PH-A

The dark red-colored WST-1 reagent (2-(4-iodophenyl)-3-(4-nitrophenyl)-5-(2,4-disulfophenyl)-2H-tetrazolium, monosodium salt), was used to monitor PH-A toxicity on MCF-7 cells. The cells were placed in a 96-well culture plate ($20 \times 10^4$ cells in each well) and the $IC_{50}$ dose of PH-A was determined using different PH-A concentrations (100–0.01 μM) with the MCF-7 cell line for 24–96 h. The number of living cells was determined by adding 20 μL cell proliferation reagent, WST-1, to each well. After 20, 40 and 60 min, yellow-colored formazan salt was formed and the absorbance was measured in a micro plate reader (Thermo) at 450/630 nm. Then the percentage of cytotoxicity was calculated.

#### 2.8.2. Intracellular uptakes of $^{99m}$Tc-PH-A and $^{99m}$Tc-PH-A-BSANPs

The *in vitro* cellular uptake of $^{99m}$Tc labeled PH-A and PH-A-BSANPs was performed using the MCF-7 cell line. MCF-7 cells were placed in 24-well culture plates ($1 \times 10^6$ cells in each well). The cells were rapidly washed three times with 0.9% NaCl. $^{99m}$Tc-PH-A and $^{99m}$Tc-PH-A-BSANPs were added to the cells in the RPMI-1640 and counted with a Cd(Te) detector equipped with a RAD 501 single channel analyzer. The cells were incubated for 10, 30, 60, 90 and 120 min at 37 °C in darkness. The same amount of PH-A was used for $^{99m}$Tc-PH-A and $^{99m}$Tc-PH-A-BSANPs (4 μg) to observe the efficiency of bovine serum albumin nanoparticles on uptake into the cell. Specific activity was determined to be an average of 0.022 GBq/μmol for each well. At the end of the incubation times the $^{99m}$Tc-PH-A and $^{99m}$Tc-PH-A-BSANPs were removed and then the cells were washed three times with 0.9% NaCl solution to eliminate the free $^{99m}$Tc and other free materials. The radioactivity of each well was again counted with a Cd(Te) detector.

### 2.9. Statistical analysis

Differences in the mean values of measured activities were evaluated statistically using the SPSS 16.0 program (Univariate Variance Analyses and Pearson Correlation). Probability values of $p < 0.05$ were considered to be significant.

## 3. Results and discussion

### 3.1. NMR, UV–vis spectrometry and mass spectrometry

The chemical structure of PH-A was checked with $^1$H NMR and MS (ESI). UV ($CH_2C1_2$) $\lambda_{max}$: 666 (0.36), 610 (0.06), 538 (0.063), 508 (0.07), 412 (0.79), $^1$H NMR (400 MHz, $CDCl_3$) $\delta$ ppm: 9.57 (s, 1H, CH-5), 9.45 (s, 1H, CH-10), 8.64 (s, 1H, CH-20), 7.99 (q, 1H, $J$ = 6.4 Hz, $3^1$), 6.25, 6.19 (q, 1H + 1H, $J$ = 16.8 Hz, $3^2$), 5.25, 5.14 (d, 1H + 1H, $J$ = 20 Hz, $13^2$-$CH_2$), 4.51 (dq, 1H, $J$ = 2 Hz, CH-18), 4.32 (dt, 1H, $J$ = 8.4 Hz, CH-17), 3.67 (s, 3H, $COOCH_3$), 3.61 (s, 3H, $CH_3$-$12^1$), 3.55 (q, 2H, $J$ = 8 Hz, $CH_2$-$8^1$), 3.41 (s, 3H, $2^1$-$CH_3$), 3.23 (s, 3H, $CH_3$-$7^1$), 2.58–2.55, 2.34–2.27 (m, 2H + 2H, 17-$CH_2CH_2$), 1.83 (d, $J$ = 7.2 Hz, $CH_3$-$18^1$), 1.67 (t, $J$ = 7.6 Hz, $CH_3$-$8^2$), −0.37, −2.07 (br, 1H + 1H, NH). MS (ESI): m/z for $C_{34}H_{36}N_4O_3$ $(M+H)^+$: 548. PH-A (Fig. 1) (Ocakoglu et al., 2011).

### 3.2. Characterization of BSANPs and PH-A-BSANPs

#### 3.2.1. Determination of particle size, zeta potential and morphology

The size of the BSANPs and PH-A-BSANPs was determined to be in the range 190–210 nm by DLS and SEM (Fig. 1). The loading of PH-A slightly increased the size of the BSANPs. Particle size and size distribution are the most important characteristics of colloidal drug delivery systems. Organ distribution and tumor targeting efficiency are affected by particle size. Particles with this size are suitable for use in drug delivery systems. According to the previous studies, if the nanoparticles are smaller than 100 nm they are non-selective for most tissues and tumors. Moreover, smaller nanoparticles have aggregation problems when they are delivered into the target tissue and they can move into the blood capillaries. However, larger particles can be more quickly eliminated from the blood (Cho et al., 2008; Chen et al., 2009; Wacker et al., 2010).

According to the SEM images (Fig. 1), the nanoparticles are highly monodisperse and near-spherical, although there are no

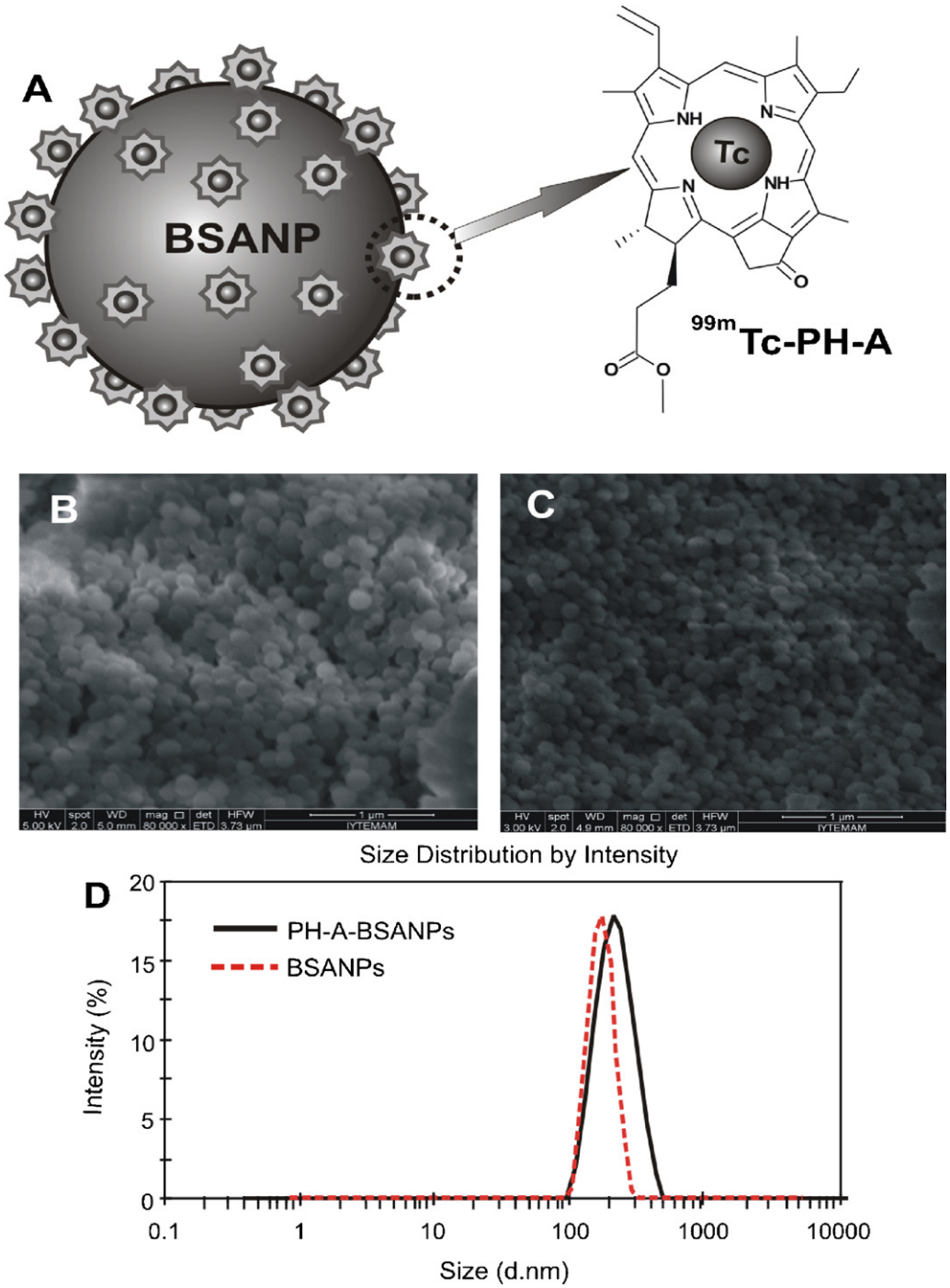


**Fig. 1.** (A) Schematic illustration of $^{99m}$Tc-PH-A complex (right) attached BSA nanoparticles for use as a cancer targeting agent (left). (B and C) SEM images of a representative BSANPs and PH-A-BSANPs, respectively. (D) Particle size distribution of BSANPs (dashed line) and PH-A-BSANPs (solid line).

changes in SEM images in the appearance of BSANPs before and after PH-A loading.

The significant increases were observed in the zeta potential from −52.3 mV to −36.6 mV for BSANPs and PH-A-BSANPs, respectively. These results indicate that the loading of PH-A caused changes in the surface potential of BSA nanoparticles (Yang et al., 2010; Wacker et al., 2010). Zeta potential is quite important for colloids and nanoparticles in suspension. Its value is closely related to suspension stability and particle surface morphology. Therefore, it is widely used to explain adsorption or derivatization of active materials with nanoparticles (Mohanraj and Chen, 2006; Yang et al., 2010). In our study, the zeta potential of the BSANPs was −52.3 mV and changed to −36.6 mV after adsorption with PH-A. This change in the zeta potential of BSANPs is indicative of successful adsorption with PH-A.

### 3.3. Photophysical properties of the PH-A-BSANPs

It is possible to see an almost identical pattern for emission spectra as well. For easy comparison, PH-A and PH-A-BSANPs in solution were also shown in Fig. 2. The maximum for PH-A loaded BSANPs (PH-A-BSANPs) slightly shifts to 678 nm compared to that

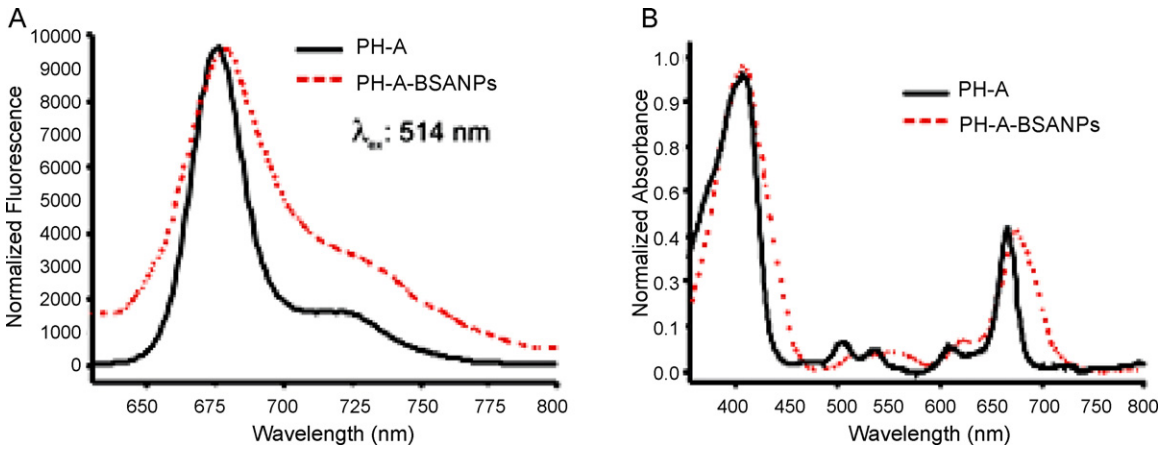


**Fig. 2.** Steady-state fluorescence (A) and UV–vis absorption spectra (B) of PH-A (solid line) and PH-A-BSANPs (dashed line) measured in ethanol. Data are normalized at Soret band maximum.

of PH-A at 673 nm. These observations can be considered as a first indication of dye aggregation processes inside or on the surface of nanoparticles.

The absorption spectra of PH-A and PH-A-BSANPs in ethanol can be seen in Fig. 2. It reveals a pronounced bathochromic shift in the $Q_y$ band from 665 nm (PH-A in solution) to 674 nm (PH-A-BSANPs). This shift is very characteristic for PH-A whenever it is attached to large molecules such as dendrimers or nanoparticles (Wacker et al., 2010).

The efficiency of adsorption of PH-A on BSANPs surface was determined according to the UV–vis absorption measurements (λ: 670 nm). The amount of unabsorbed PH-A in wash water was determined and the efficiency of adsorption was found to be 97 ± 2.3%.

PH-A was successfully loaded onto non-covalent BSA nanoparticles and this complex remained stable during the *in vivo* and *in vitro* studies. In the study carried out by Chen et al. Pheo molecules were loaded on HSA nanoparticles by non-covalent drug adsorption. And they indicated that PH-A-BSANPs are stable for several days without losing their photophysical properties (Chen et al., 2009). Wacker et al. demonstrated that the drugs were adsorbed to HSA nanoparticles. As it is known drugs can be incorporated within the particle matrix, absorbed on the particle surface or bound by covalent linkage. The adsorption binding has an advantage which can be indicated in a fast drug release from the carrier leading to a high activity in terms of photosensitization (Wacker et al., 2010).

### 3.4. Quality controls of radiolabeling

The labeling efficiency of PH-A was determined using the RTLC method. $R_f$ values of reduced $^{99m}$Tc and $^{99m}$Tc-PH-A were determined to be 0.85 and 0.05 by RTLC respectively when mobile phase 1 (ACD) was used. For mobile phase 2 (methanol/water, 4:1) the $R_f$ values of reduced $^{99m}$Tc and $^{99m}$Tc-PH-A were 0.01 and 0.5, respectively. Radiolabeling yields of $^{99m}$Tc-PH-A at the reaction condition, 100 μg $SnCl_2$, pH 7, 60–70 °C, 25 min, were determined as 90 ± 3.2% (Ocakoglu et al., 2011).

The radiochemical purity of $^{99m}$Tc-PH-A-BSANPs was found to exceed 90 ± 1.2% as seen in Fig. 3. According to the results, a very small amount of the radioactivity was passed into the supernatant. The stability of $^{99m}$Tc-PH-A-BSANPs was tested in pH 7 PBS shaking continually. The stability results show that approximately 1–2% of radioactivity was determined in the upper phase over incubation. According to the results, $^{99m}$Tc-PH-A-BSANPs remained stable during incubation at 37 °C for up to 120 min in pH 7 PBS.

In aqueous solution technetium can exist in any oxidation state (OS) from +VII to +I, but the most stable OS are +IV and +VII. The OS is considered to be one of the main parameters determining the chemical nature of the complexes. Reduced $^{99m}$Tc can easily form chemical bonds with electron donor atoms, such as oxygen, nitrogen and sulfur in order to get a technetium complex. In our study, the radiolabeling efficiency of $^{99m}$Tc-PH-A was found to be 90 ± 3.2% according to the chromatograms (Ocakoglu et al., 2011). In the previous studies, PH-A and some photosensitizers similar to PH-A (T3, 4BCPC, Photosan-3) were labeled with $^{99m}$Tc. Moreover, Smith et al. used different metal complexes of PH-A (Ni, Cu, Zn etc.), and Yang et al. prepared $^{99m}$Tc-hematoporphyrin linked albumin nanoparticles (Smith et al., 1985; Yang et al., 2010).

### 3.5. Biodistribution results

*In vivo* organ distribution of $^{99m}$Tc-PH-A-BSANPs and $^{99m}$Tc-PH-A were performed using female Albino Wistar rats. According to the biodistribution results (Fig. 4), the uptake of $^{99m}$Tc-PH-A-BSANPs reached also a high in the kidney (%ID/g: 0.340, $p < 0.05$), large intestine (%ID/g: 0.966, $p < 0.05$), breast (%ID/g: 0.188, $p < 0.05$) and uterus (%ID/g: 0.262, $p < 0.05$) at 120 min.

As seen in Fig. 4(B), the uptake of $^{99m}$Tc-PH-A in kidney (1.43%ID/g, $p < 0.05$) and l. intestine (1.10%ID/g, $p < 0.05$) reached the highest values at 60 min after post injection. In contrast, the uptake was low in ovary, breast and uterus during the experimental period. According to the data in Fig. 4(B), the uptake of $^{99m}$Tc-PH-A in ovary and uterus was maximum at 120 min after the

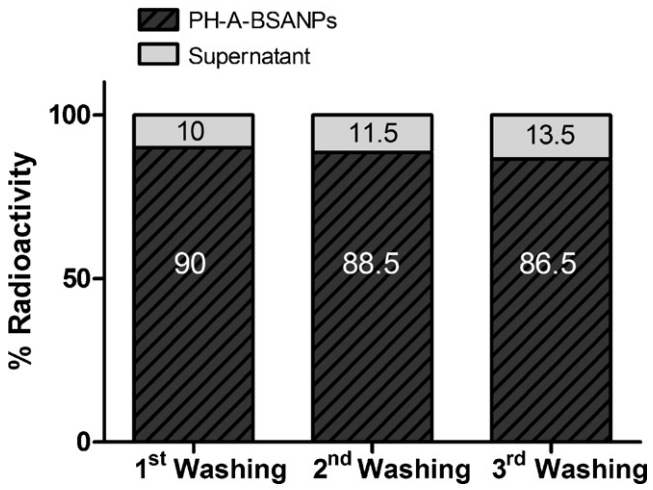


**Fig. 3.** Radiolabeling results of PH-A-BSANPs.

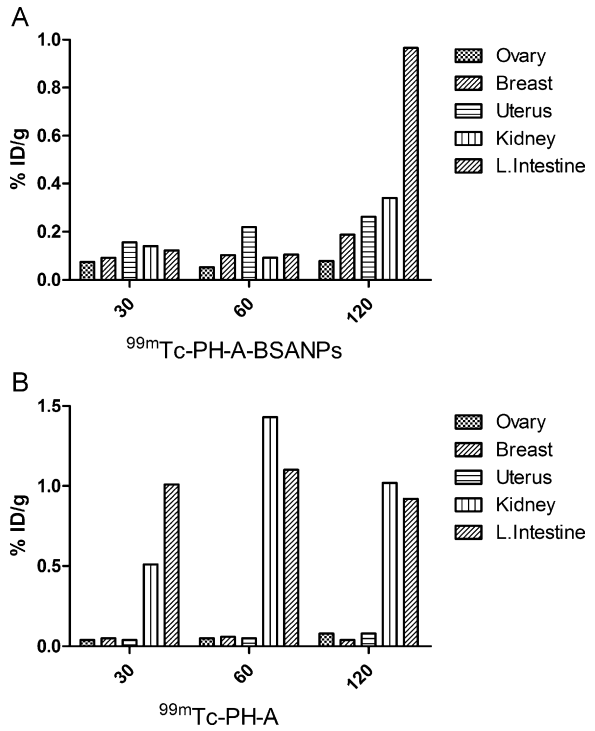


**Fig. 4.** Biodistribution results of $^{99m}$Tc-PH-A-BSANPs (A) and $^{99m}$Tc-PH-A (B).

administration of the compound. The uptake values were measured in the order of %ID/g: 0.02 ($p < 0.05$) and 0.05 ($p < 0.05$), respectively. On the other hand, the radiolabeled PH-A uptake reached maxima at 60 min in breast (%ID/g: 0.03, $p < 0.05$). Our results demonstrated that, $^{99m}$Tc-PH-A-BSANPs have a significant uptake in the uterus and breast at 120 min due to the fact that PH-A has a high affinity for these organs. At the same time, it was demonstrated that the uptake of $^{99m}$Tc-PH-A-BSANPs was almost the same after 30 min. While the elimination of $^{99m}$Tc-PH-A-BSANPs carried out by the urinary system organs, there was an increased uptake of $^{99m}$Tc-PH-A-BSANPs in the breast and uterus at 120 min. These results indicated that $^{99m}$Tc-PH-A show localization potential for the breast and uterus and BSANPs increased uptake of $^{99m}$Tc-PH-A in these organs. In summary, $^{99m}$Tc-PH-A-BSANPs showed good localization in uterus and breast.

The clearance of $^{99m}$Tc-PH-A-BSANPs and $^{99m}$Tc-PH-A from the body were occurred via urinary system organs (kidney and l. intestine). Other studies also proved that many photosensitizers similar to PH-A, such as T3, 4BCPC, Photosan-3, were removed from body via urinary system (Murugesan et al., 2002; Aprahamian et al., 1993).

On the other hand, it is reported by Yang. et al. that $^{99m}$Tc-hematoporphyrin linked albumin nanoparticles ($^{99m}$Tc-HP-ANP) indicated very different pharmacokinetic properties than $^{99m}$Tc-hematoporphyrin ($^{99m}$Tc-HP), and $^{99m}$Tc-HP was uptake in the body after injection and excreted rapidly via the kidneys. They show that the formulation with nanoparticle affect the retention time of hematoporphyrin (Yang et al., 2010). We obtained similar results to theirs.

### 3.6. Cell culture studies on MCF-7 cell line

#### 3.6.1. Cytotoxicity assay

According to WST-1 cytotoxicity test results, the cell 50% viability was observed at a concentration of 25 μM PH-A. $IC_{50}$ value of PH-A has been accepted as 25 μM for MCF-7 cell line. Conversely, BSA is a common protein in plasma, and it is non-toxic and non-antigenic (Chen et al., 2009; Kratz, 2008). Consequently, in this study, the cytotoxicity experiment in the MCF-7 cell line was performed only for PH-A.

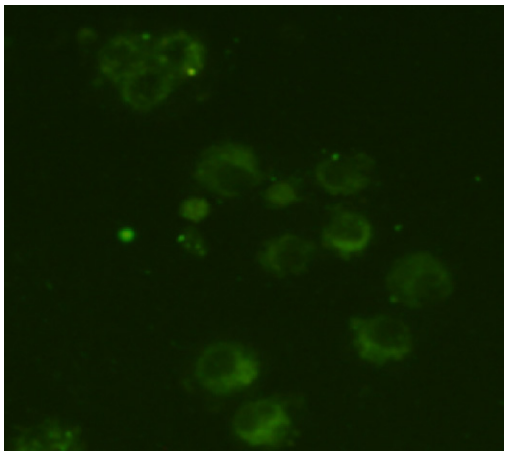

**Fig. 5.** Fluorescence microscopy image of PH-A-BSANPs inside MCF-7 cells.

#### 3.6.2. The uptake of $^{99m}$Tc-PH-A and $^{99m}$Tc-PH-A-BSANPs in MCF-7 cell line

As seen in Fig. 5. PH-A-BSANPs penetrated inside the MCF-7 cells. Furthermore, the results for the cellular uptake of both the $^{99m}$Tc-PH-A and $^{99m}$Tc-PH-A-BSANPs are shown in Fig. 6. Our results demonstrated that $^{99m}$Tc-PH-A-BSANPs showed an efficient uptake compared to $^{99m}$Tc-PH-A in human breast tumor cells.

The MCF-7 breast cancer cell model was used for *in vitro* evaluation of $^{99m}$Tc-PH-A-BSANPs. According to the results of the cell culture studies, $^{99m}$Tc-PH-A showed a similar uptake to $^{99m}$Tc-PH-A-BSANPs within 10 min. Conversely, in the other stages of incubation the localization of $^{99m}$Tc-PH-A and $^{99m}$Tc-PH-A-BSANPs changed during incubation. This situation can be explained by the presence of different mechanisms of penetration of PH-A and BSANPs-PH-A into the cell. Accordingly, PH-A penetrates from the membrane into the cell by diffusion due to its low molecular weight. Conversely, $^{99m}$Tc-PH-A-BSANPs are localized into the cells by endocytosis (Chen et al., 2009). The results obtained show that the intracellular uptake of $^{99m}$Tc-PH-A-BSANPs is significantly more efficient than the intracellular uptake of $^{99m}$Tc-PH-A. In a previous study, Yang et al. demonstrated that, $^{99m}$Tc-HP-ANP increased

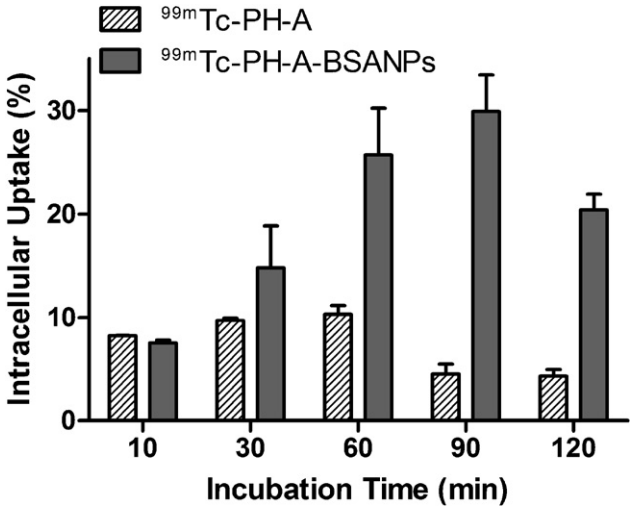


**Fig. 6.** Intracellular uptake of $^{99m}$Tc-PH-A and $^{99m}$Tc-PH-A-BSANPS in MCF-7 cells after different incubation times.

penetration in murine lung tumors, which was induced by CT-26 colon cancer cells, compared to normal lungs. As a result, albumin nanoparticles increased the accumulation of hematoporphyrin in cell lines, and $^{99m}$Tc-HP-ANP demonstrated good radioimaging properties according to the scintigraphic application in rabbits (Yang et al., 2010). In another study related to PH-A loaded human serum albumin nanoparticles (PHSA), after 24 h incubation in Jurkat cells, PHSA showed a higher phototoxicity than Pheo (Chen et al., 2009). Obtained are similar to their results.

## 4. Conclusions

In this study, BSANPs were prepared by a desolvation method and a photosensitizer (PH-A) was successfully loaded onto the nanoparticles' surface. The size of the particles was measured in the range from 190 to 210 nm. The biodistribution of $^{99m}$Tc-PH-A-BSANPs in healthy female rats showed high uptake in the breast and uterus. $^{99m}$Tc-PH-A-BSANPs might therefore be used in scintigraphic tumor imaging for the organs. $^{99m}$Tc-PH-A-BSANPs were taken up to human breast adenocarcinoma cell line (MCF-7). $^{99m}$Tc -PH-A-BSANPs showed a higher cellular uptake compared to $^{99m}$Tc-PH-A in the cell line. Moreover, BSANPs may increase the ability of PH-A to target tumor cells. Hence, side effects and unwanted chemical reactions are kept to a minimum, and PH-A is protected from *in vivo* degradation. The result of the studies are significantly encouraging enough to bring about further evaluation of radiolabeled photosensitizer linked BSANPs as a possible imaging agent for breast and uterus tumors. In conclusion, $^{99m}$Tc-PH-A-BSANPs are suitable for imaging and drug delivery in the field of nanomedicine, and may be used as site-specific tumor imaging agent.

## Acknowledgement

The authors gratefully acknowledge the financial support received from the Department of Scientific Projects at Ege University, Izmir, Turkey (Project no: 2010-NBE-003).

## References

Aprahamian, M., Evrard, S., Keller, P., Tsuji, M., Balboni, G., Damge, C., Marescaux, J., 1993. Distribution of pheophorbide A in normal tissues and in an experimental pancreatic cancer in rats. Anticancer Drug Des. 8, 101–114.

Babbar, A.K., Singh, A.K., Goel, H.C., Chauhan, U.P.S., Sharma, R.K., 2000. Evaluation of $^{99m}$Tc-labeled photosan-3, a hematoporphyrin derivative, as a potential radiopharmaceutical for tumor scintigraphy. Nucl. Med. Biol. 27, 419–426.

Chatterjee, D.K., Fong, L.S., Zhang, Y., 2008. Nanoparticles in photodynamic therapy: an emerging paradigm. Adv. Drug Deliv. Rev. 60, 1627–1637.

Chen, K., Preuß, A., Hackbarth, S., Wacker, M., Langer, K., Röder, B., 2009. Novel photosensitizer-protein nanoparticles for photodynamic therapy: photophysical characterization and *in vitro* investigations. J. Photochem. Photobiol. B 96, 66–74.

Cho, K., Wang, X., Nie, S., Chen, Z.G., Shin, D.M., 2008. Therapeutic nanoparticles for drug delivery in cancer. Clin. Cancer Res. 14, 1310–1316.

Crommelin, D.J.A., Schreier, H., 1994. Colloidal drug delivery systems. In: Kreuter, J. (Ed.), Nanoparticles. Marcel Dekker Inc., New York, Basel and Hong Kong, pp. 219–342.

Hans, M.L., Lowman, A.M., 2002. Biodegradable nanoparticles for drug delivery and targeting. Curr. Opin. Solid State Mater. Sci. 6, 319–327.

Huber, V., Sengupta, S., Würhtner, F., 2008. Structure–property relationships for self-assembled zinc chlorine light-harvesting dye aggregates. J. Eur. Chem. 14, 7791–7807.

Jori, G., Fabris, C., Soncin, M., Ferro, S., Coppellotti, O., Dei, D., Fantetti, L., Chiti, G., Roncucci, G., 2006. Photodynamic therapy in the treatment of microbial infections: basic principles and perspective applications. Lasers Surg. Med. 38, 468–481.

Josefsen, L.B., Boyle, R.W., 2007. Photodynamic therapy and the development of metal-based photosensitizers. Hindawi Pub. Corp., doi:10.1155/2008/276109.

Jun, J.Y., Nguyen, H.H., Paik, S.Y.R., Chun, H.S., Kang, B.C., Ko, S., 2011. Preparation of size controlled bovine serum albumin (BSA) nanoparticles by a modified desolvation method. Food Chem. 127, 1892–1898.

Keller, P., Sowinska, M., Tassetti, V., Heisel, F., Hajri, A., Evrard, S., Miehe, J.A., Marescaux, J., Aprahamia, M., 1996. Photodynamic imaging of a rat pancreatic cancer with pheophorbide. J. Photochem. Photobiol. 63, 860–867.

Kratz, F., 2008. Albumin as a drug carrier: design of prodrugs, drug conjugates and nanoparticles. J. Control. Release 132, 171–183.

Labhasetwar, V., Song, C., Levy, R.J., 1996. Nanoparticle drug delivery system for restenosis. Adv. Drug Deliv. Rev. 24, 63–85.

Langer, K., Balthasar, S., Vogel, V., Dinauer, N., Von Briesen, H., Schubert, D., 2003. Optimization of the preparation process for human serum albumin (HSA) nanoparticles. Int. J. Pharm. 257, 169–180.

Lin, W., Garnett, M.C., Schacht, E., Davis, S.S., Illum, L., 1999. Preparation and *in vitro* characterization of HSA-mPEG nanoparticles. Int. J. Pharm. 189, 161–170.

Mohanraj, V.J., Chen, Y., 2006. Nanoparticles – a review. Trop. J. Pharm. Res. 5, 561–573.

Murugesan, S., Shetty, S.J., Srivastava, T.S., Samuel, A.M., Noronha, O.P.D., 2002. Preparation and biological evaluation of the new chlorine photosensitizer T3, 4BCPC for detection and treatment of tumors. J. Photochem. Photobiol. B 68, 33–38.

Ocakoglu, K., Bayrak, E., Onursal, M., Yilmaz, O., Yurt Lambrecht, F., Holzwarth, A.R., 2011. Evaluation of $^{99m}$Tc-Pheophorbide-*a* use in infection imaging: a rat model. Appl. Radiat. Isot. 69, 1165–1168.

Ofokansi, K., Winter, G., Fricker, G., Coester, C., 2010. Matrix-loaded biodegradable gelatin nanoparticles as a new approach to improve drug loading and delivery. Eur. J. Pharm. Biopharm. 76, 1–9.

Sharman, W.M., Van Lier, J.E., Allen, C.M., 2004. Targeted photodynamic therapy via receptor mediated delivery systems. Adv. Drug Deliv. Rev. 56, 53–76.

Smith, K.M., Goff, D.A., Simpson, D.J., 1985. Meso substitution of chlorophyll derivatives: direct route for transformation of bacteriopheophorbides d into bacteriopheophorbides. J. Am. Chem. Soc. 107, 4946–4954.

Wacker, M., Chen, K., Preuss, A., Possemeyer, K., Roeder, B., Langer, K., 2010. Photosensitizer loaded HSA nanoparticles. I: preparation and photophysical properties. Int. J. Pharm. 393, 253–262.

Wang, G., Kucharski, C., Lin, X., Uludag, H., 2010. Bisphosphonate-coated BSA nanoparticles lack bone targeting after systemic administration. J. Drug Target. 18, 611–626.

Weber, C., Kreuter, J., Langer, K., 2000. Desolvation process and surface characteristics of HSA-nanoparticles. Int. J. Pharm. 196, 197–200.

Yang, S.G., Chang, J.E., Shin, B., Park, S., Na, K., Shim, C.K., 2010. $^{99m}$Tc-hematoporphyrin linked albumin nanoparticles for lung cancer targeted photodynamic therapy and imaging. J. Mater. Chem. 20, 9042–9046.

Zhang, L., Hou, S., Mao, S., Wei, D., Song, X., Lu, Y., 2004. Uptake of folate-conjugated albumin nanoparticles to the SKOV3 cells. Int. J. Pharm. 287, 155–162.